# Sub-basalt imaging in the Faroe-Shetland Basin using CSEM&MT data to constrain the velocity model

*Martin Panzner* and Wiktor Waldemar Weibull, Department for Petroleum Technology and Applied Geophysics, NTNU, and Jan Petter Morten, EMGS ASA*



## SUMMARY

In this study we demonstrate how incorporating controlled source electromagnetic (CSEM) and magnetotelluric (MT) data in the velocity model building improves seismic depth imaging in sub-basalt settings. We consider data acquired in the Faroe-Shetland basin. The resistivity model obtained from inversion of the electromagnetic (EM) data provides information about sub-basalt structure and resistivity. The EM data can image both the thickness and the extent of basalt layers, as well as the sediments underneath. We update the velocity model using a correlation between resistivity and seismic velocity derived from nearby well data. Our reverse-time migration (RTM) imaging improvements demonstrate the advantage of this integrated approach.

## INTRODUCTION

Sub-volcanic sediments can be hydrocarbon bearing, but are difficult to image with seismic. Much of the seismic energy is reflected at the top basalt interface due to the large seismic impedance contrast. An additional difficulty are interbed multiples which develop as a result of interchanging layers of basalt and other rock types, such as volcanoclastics. These layers can have very different seismic properties which leads to multiple internal reflections and scattering. Seismic sub-basalt imaging challenges have been addressed by several approaches, and important improvements for imaging of the base of the basalt layer as well as sub-basalt strata have been published. For instance Fruehn et al. (2001) and White et al. (2003) used long offset first arrivals for travel-time tomography in order to determine the sub-basalt velocities. However, the resulting velocity models lack resolution, and there is remaining ambiguity in the interpretation of the base basalt and the top basement reflectors in the migrated images.

In order to obtain a successful depth migration, the velocity model must correctly determine the travel time for the reflection events. In the reverse time-migration algorithm considered in this paper (Weibull and Arntsen, 2013), the measured reflections will then correlate at the location of the impedance contrast. However, the velocity model need not incorporate sharp interfaces at the impedance contrasts as long as the travel time is described correctly. Low-frequency data which are only sensitive to large-scale structure can therefore be used to construct the velocity model. Low-frequency CSEM and MT data can be an important complement and help to improve seismic depth imaging (Colombo et al., 2013).

The CSEM and MT methods utilize electromagnetic fields to measure resistivity variations in the subsurface. Basalt is very resistive in contrast to sediments, which makes EM methods

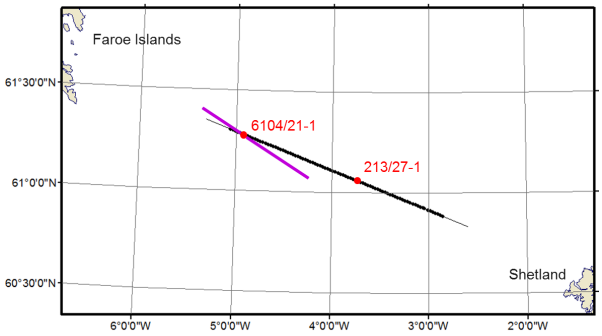


Figure 1: Map showing the location of CSEM and MT receivers (black), the location of the FLA_06 seismic line (magenta) and the location of the wells at Brugdan (6104/21-1) and Rosebank (213/27-1) (red dots).

well suited for imaging the basalt layer and the transition to sub-basalt sediments. The signals used for CSEM have a much lower frequency content and longer wavelength compared to the seismic signal, and the fields are therefore not scattered in the same way by small-scale structures within the basalt. The MT source signals are part of the Earth's natural electromagnetic spectrum and have even lower frequencies than CSEM. Low-frequency EM fields have a large penetration depth and allow to delineate even deep basement structures. Herredsvela et al. (2012) and Alumbaugh et al. (2013) have shown in synthetic modeling and inversion studies that imaging using CSEM and MT data can resolve the thickness and extent of a very inhomogeneous basalt layer as well as the sediments below. Both the structural information and the quantitative resistivity distribution, recovered by the EM methods, can be used to update and improve the velocity model for seismic depth imaging. We demonstrate an integrated seismic and EM imaging approach using data from a regional seismic 2D survey and an EM survey. The data were acquired in the Faroe-Shetland Basin, and the survey layouts are shown in Figure 1.

The development of the Faroe-Shetland basin is strongly influenced by the breakup of the North Atlantic, followed by extensive magmatism in the Paleocene and Eocene age. Extrusive igneous rocks dominate the North-West margin of the basin. The volcanic complex is a succession of volcanoclastics at the base, a mix of volcanoclastics and flow basalts in the middle, and thick flow-basalts at the top. The thickness of the volcanic sequence decreases towards South-East.



DOI http://dx.doi.org/10.1190/segam2014-0715.1

## CSEM AND MT DATA PROCESSING AND IMAGING

The CSEM and MT survey was acquired during autumn 2011. We utilize a part of the survey data constituting a long, regional 2D-line. The 2D line ranges from the East Faroe High in the NW over the Corona Basin and the Corona Ridge to the Flett Sub-Basin in the SE. Both the Brugdan (6104/21-1) well and the Rosebank (213/27-1) well are situated along this line.

Robust multi-station processing (Egbert, 1997) was used to prepare the MT data. We carried out CSEM and MT data inversion using a Gauss-Newton type joint inversion scheme with a finite element forward modeling operator (Key and Ovall, 2011). No constraints were applied in the inversion, so the imaging result shown in Figure 2 is purely data driven. Still, the resistivity image is consistent with the resistivity values and the reported top and base of basalt from the two wells at Brugdan and Rosebank. Moreover, the top of the resistive basalt layer is consistent with the depth to the top-basalt reflector from seismic depth imaging along the entire seismic line.

Hoversten et al. (2013) carried out an EM imaging study using the same data, and obtained results similar to Figure 2. In this study we go on to use the EM resistivity model to update the seismic velocity model. We utilize both the structural definition as well as the quantitative resistivity information. We will show that this approach improves the seismic depth-imaging result significantly. The survey layouts for the seismic line and the CSEM and MT line overlap only partly, therefore only a subset of the resistivity model was used. The area of overlap is indicated by the dashed line in Figure 2.

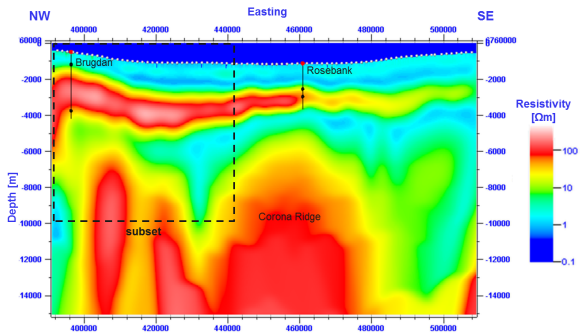


Figure 2: Resistivity model from the CSEM and MT joint inversion. The extent of this section corresponds to the entire EM survey line. The resistivity scale is such that the basalt and the deep basement structures appear in red, while the more conductive sediments above and below the basalt are appear in blue and green colors.

## WELL LOG ANALYSIS

We analyzed the relation between the acoustic velocity from the sonic log and the resistivity from the laterolog in the Brugdan well (6104/21-1). There is a clear correlation between the two parameters as seen in Figure 3. A linear relationship describes the correlation between velocity and the logarithm of resistivity for velocities $< 5000$ m/s. For higher velocities the relation approaches an asymptotic behavior. The reason for this transition is most likely a change in the rock properties that determine the rock physics relationship between the two parameters. For low velocities and resistivities the relation is mainly controlled by the porosity, tortuosity and the pore fluid resistivity. But for high velocities and resistivities the relation becomes a function of the matrix properties and composition of the rock.

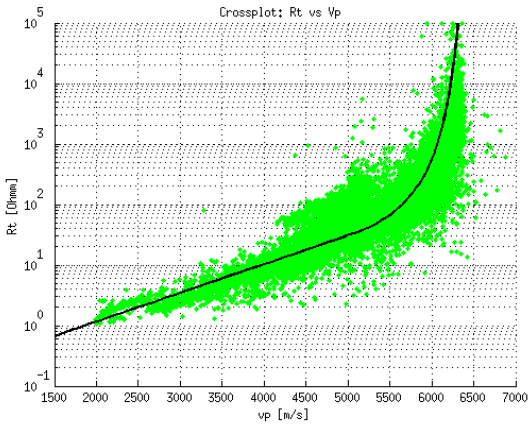


Figure 3: Cross-plot of sonic log acoustic velocity, and laterolog resistivity from the Brugdan well (6104/21-1). The trend in Equation (1) is shown as a black line.

In this work, we did not use specific rock physics models to describe the correlation between resistivity, $\rho$, and velocity, $v_p$. For our purpose it is sufficient to find a mathematical description of the relation between $\rho$ and $v_p$ without further classification of the rock properties. Curve fitting was used to derive the following relation:

$$v_p(\rho) = \begin{cases} 2118 \cdot \log_{10}(\rho) - 1869.5, & \text{if } v_p < 5000 \text{ m/s} \\ \frac{-1239}{\log_{10}(\rho) - 0.701} + 6604, & \text{if } v_p \geq 5000 \text{ m/s}. \end{cases} \quad (1)$$

For the rocks penetrated by the well, this relationship represents a calibrated transformation from resistivity into velocity. There is limited penetration into the sedimentary rock below basalt, so the relationship can be assumed less accurate for such rocks. Due to the fact that only one well log was available we will not be able to capture lateral variations in the basalt layer. Note that due to the large dynamical range of resistivity as compared to velocity, the uncertainty in the transformation from resistivity to velocity, $\delta v_p(\rho)/v_p$, is smaller than the uncertainty of the opposite transformation from velocity to resistivity, $\delta\rho(v_p)/\rho$.

We will use the empirical relationship in (1) to convert the resistivity model from CSEM and MT data inversion into a seismic velocity model. The relationship $v_p(\rho)$ was calibrated on well-log data that was measured on a much finer spatial scale than the resolution of the seismic data and in particular the EM data. In principle a proper up-scaling should have been applied to the well data before we determined the relationship $v_p(\rho)$.



DOI http://dx.doi.org/10.1190/segam2014-0715.1

Such up-scaling would represent the measurement on the scale of the seismic and EM data. For the present study we make the assumption that such up-scaling operations lead to a similar relationship $v_p(\rho)$ with $v_p$ and $\rho$ on the scales of the seismic and the EM data.

## SEISMIC DATA PROCESSING AND IMAGING

We utilized data from a 2D seismic line (FLA_06) of the Faroes Large Aperture Research Experiment (FLARE) (Fruehn et al., 1998). Long-offset data was acquired in a two-vessel operation, where each vessel was shooting towards the other. The data was organized in so-called super gathers with up to 18 km offset and was compressed to 100 m hydrophone group spacing and 100 m shot spacing. The seismic line has an angle of 10 degrees to the CSEM&MT line, and crosses the Brugdan well (6104/21-1) location as shown in the survey layout in Figure 1.

For the depth imaging we used only the direct reflection data with offsets less then 6 km. Prior to the depth imaging, the data was processed using the following steps: source estimation and deconvolution; semblance analysis; multiple attenuation using radon; low-pass filter (30 Hz); top mute and inner mute. A major challenge with this data set is to tackle the strong multiples from the large seismic impedance contrast at the top basalt interface, which also appear as second-order multiples from the water bottom. Radon based de-multiple strategies worked well in the deep water section towards SE were the data have sufficient stacking power and good moveout separation between primaries and multiples. However, in the shallow water part towards the NW of the line, there were few usable traces with sufficient moveout separation so that the multiple suppression was only partly successful. Inter-bed multiples from within the basalt cannot be attenuated using velocity based de-multiple techniques.

Seismic imaging in the presence of basalt is challenging for the reasons described in the introduction. In addition, the subsurface structures can have complicated geometries, which in combination with strong velocity variations can cause complicated ray paths. In order to still achieve good imaging results, we utilized a 2D reverse time migration (RTM) developed at the Norwegian University of Science and Technology - NTNU (Weibull and Arntsen, 2013).

A first velocity model was built using a standard approach where the velocities down to the top basalt reflector are found by semblance analysis. Below the top basalt reflection, it was difficult to properly pick velocities since the reflections are weak. Therefore we just extrapolated the sediment velocities linearly. The RMS-velocities were then converted into interval velocities using the Dix equation. Depth migrated angle gathers show flat reflectors down to the top of basalt, which give us confidence that the velocity model for the basalt overburden is correct. The only purpose of this migration run was to accurately determine the depth to the top basalt interface for further velocity model building.

A second velocity model was built by flooding the model below the picked top basalt interface. We used a constant velocity of 4900 m/s. This velocity approximates the basalt velocity which was found by analyzing the slope of the refracted waves, as well as the average of the velocities in the sonic log from the nearby Brugdan well. The resulting migrated image (Figure 4a) shows some continuous reflectors at the basalt base and below. However, they are difficult to interpret and not clear enough to be used for updating the sub-basalt velocity structure. Furthermore, the sub-basalt reflections, where present, appear at small reflection angles and have too little moveout to be used for velocity analysis. Therefore we did not pursue it any further.

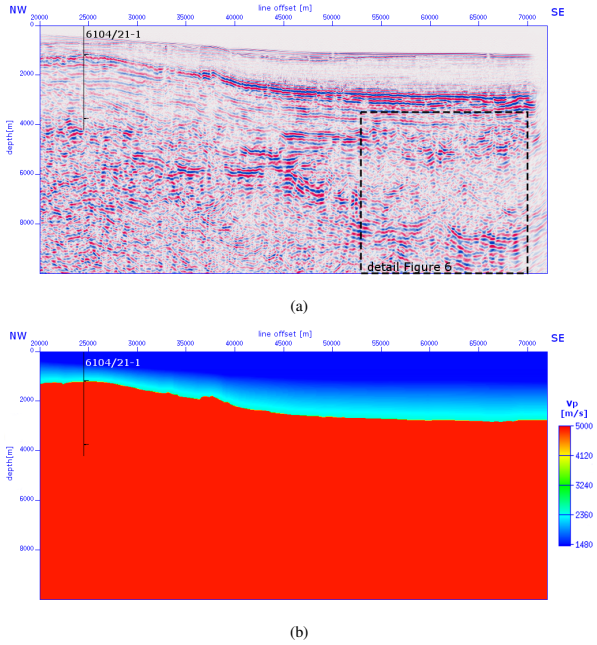


Figure 4: Top image (a) shows the RTM result when using the flooded basalt velocity model (b). The location of the Brugdan well (6104/21-1) and the top and base of basalt are indicated in black.

To update the velocity model below the top basalt interface, we now turn to the complementary information provided by CSEM and MT inversion. The correlation found in the nearby well (Equation 1) was used to convert the resistivity into seismic velocity. Since the EM line is not exactly co-located with the seismic line, we had to project the model into the seismic line. This implies the assumption that the subsurface structures are 2D with a strike direction NNE to SSW. The velocity model and the migrated seismic image are shown in Figure 5. A more detailed comparison of a specific sub-basalt reflection event is shown in Figure 6. The reflectors denoted A,A' as well as B,B' are much more focused and continuous after updating the sub-basalt velocity model.

In addition to improving the velocity model, the resistivity data can enhance the definition of often unclear sub-basalt reflectors by co-rendering the migrated seismic image and the resistivity model. The two independent data types, CSEM&MT and seismic, give complementary information about the sub-



DOI http://dx.doi.org/10.1190/segam2014-0715.1

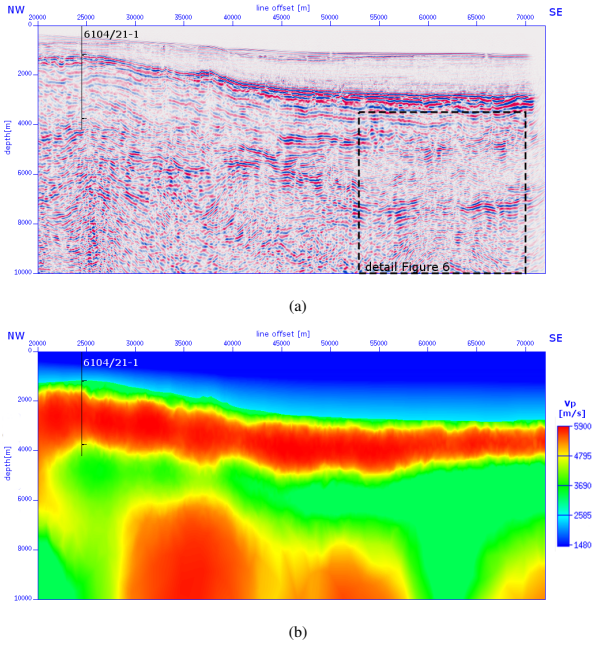


(a) (b)

Figure 5: Top image (a) shows the RTM result when using the velocity model that is based on the resistivities from CSEM and MT inversion (b). The location of the Brugdan well (6104/21-1) and the top and base of basalt are indicated in black.

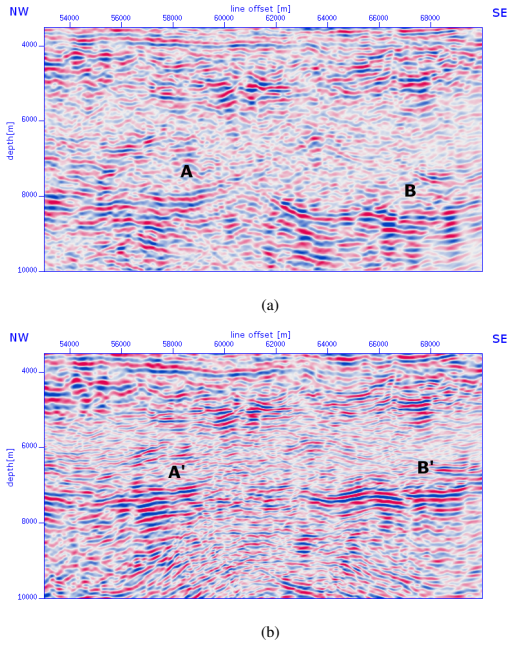


(a) (b)

Figure 6: Zoom-in on a detail of the RTM result using the flooded basalt velocity model (a) and for the updated velocity model based on the resistivities from CSEM and MT inversion (b). Imaging improvements at reflectors A,A' and B,B' are significant.

surface structures which enhances the interpretation. Furthermore, the quantitative resistivity information can give valuable insight into the lithology type.

## DISCUSSION AND CONCLUSIONS

We show that seismic depth imaging can be significantly improved by incorporating complementary data from CSEM and MT surveys. The integrated imaging results shown in this paper use information from both seismic and EM, which in combination can constrain the velocity model better. Moreover, the structural understanding and the interpretation of sub-basalt reflectors can be supported by using the resistivity information directly in the interpretation process.

One challenge with the presented work flow is that the velocity-resistivity relation must be properly calibrated to well data. Such data are typically only available for a very limited depth range and at few lateral positions. This introduces inaccuracies if the lithology varies significantly from the position of the well. If the calibration well data is insufficient to properly construct a $v_p(\rho)$ relationship then the velocity model building from resistivity could instead be based on structural interpretation directly on the resistivity model. An issue with the data sets considered here is that the orientation of the seismic and EM survey lines are not the same. At the South East end of the seismic line the maximum distance to the CSEM and MT line is 8.5 km. However, it is known that the subsurface structures in this area are more or less 2D with a strike direction NNE to SSW, which is nearly perpendicular to the headings of both the CSEM&MT and the seismic line and the effects of increasing line separation towards SE should be minor.

The improved base basalt and sub-basalt imaging demonstrated in Figure 6 can be used to improve interpretations as compared to the result from the flooded velocity model. Such improvements in sub-basalt definition could as a next step be utilized for constrained CSEM and MT inversion. For example, the updated seismic horizons could be used for structural constraints in the inversion. Such a feedback mechanism between the seismic and the EM processing is needed for a joint inversion scheme. Software which can automatically update both the resistivity and velocity models have been devised and encouraging results have been presented (Medina et al., 2012). However, the results and work flows shown in this paper demonstrate how corresponding improvements in seismic depth imaging can be achieved in a process where also the interpreter's experience can be utilized directly.

## ACKNOWLEDGMENTS

We wish to thank EMGS for the permission to publish these results. Special thanks goes to Børge Arntsen and the seismic depth imaging group at the IPT department at the Norwegian University of Science and Technology (NTNU) for fruitful discussions and giving us access to their seismic processing and imaging software. We also thank Rune Mittet for interesting discussions.

http://dx.doi.org/10.1190/segam2014-0715.1

**EDITED REFERENCES**

Note: This reference list is a copy-edited version of the reference list submitted by the author. Reference lists for the 2014 SEG Technical Program Expanded Abstracts have been copy edited so that references provided with the online metadata for each paper will achieve a high degree of linking to cited sources that appear on the Web.

**REFERENCES**

Alumbaugh, D., M. Hoversten, J. Stefani, and C. Thacher, 2013, A 3D model study to investigate EM imaging of subbasalt structures in a deepwater environment: 83rd Annual International Meeting, SEG, Expanded Abstracts, 765–769.

Colombo, D., G. McNeice, E. S. Curiel, and A. Fox, 2013, Full tensor CSEM and MT for subsalt structural imaging in the Red Sea: Implications for seismic and electromagnetic integration: The Leading Edge, **32**, 436–449, http://dx.doi.org/10.1190/tle32040436.1.

Egbert, G. D., 1997, Robust multiple-station magnetotelluric data processing: Geophysical Journal International, **130**, no. 2, 475–496, http://dx.doi.org/10.1111/j.1365-246X.1997.tb05663.x.

Fruehn, J., M. M. Fliedner, and R. S. White, 2001, Integrated wide-angle and near-vertical subbasalt study using large-aperture seismic data from the Faeroe-Shetland region: Geophysics, **66**, 1340–1348, http://dx.doi.org/10.1190/1.1487079.

Fruehn, J., R. White, K. Richardson, M. Fliedner, E. Cullen, C. Latkiewicz, W. Kirk, and J. Smallwood, 1998, FLARE — A two-ship experiment designed for sub-basalt imaging: 68th Annual International Meeting, SEG, Expanded Abstracts, 94–97, http://dx.doi.org/10.1190/1.1820649.

Herredsvela, J., A. Colpaert, S. Foss, A. Nguyen, K. Hokstad, S. Morten, C. Twarz, S. Fanavoll, and F. Mrope, 2012, Feasibility of electromagnetic methods for sub-basalt exploration: 82nd Annual International Meeting, SEG, Expanded Abstracts, doi: 10.1190/segam2012-0590.1.

Hoversten, G., D. Myer, K. Key, O. Hermann, R. Hobbet, and D. Alumbaugh, 2013, CSEM & MMT base basalt imaging: 75th Conference & Exhibition Incorporating Europec, EAGE-SPE, Extended Abstracts, Th 11 10, doi: 10.3997/2214-4609.20130137.

Key, K., and J. Ovall, 2011, A parallel goal-oriented adaptive finite element method for 2.5-D electromagnetic modelling: Geophysical Journal International, **186**, no. 1, 137–154, http://dx.doi.org/10.1111/j.1365-246X.2011.05025.x.

Medina, E., A. Lovatini, F. G. Andreasi, S. Re, and F. Snyder, 2012, Simultaneous joint inversion of 3D seismic and magnetotelluric data from the Walker Ridge: First Break, **30**, no. 4, 85–88.

Weibull, W., and B. Arntsen, 2013, Reverse time demigration using the extended imaging condition: 83rd Annual International Meeting, SEG, Expanded Abstracts, 4015–4020.

White, R. S., J. R. Smallwood, M. M. Fliedner, B. Boslaugh, J. Maresh, and J. Fruehn, 2003, Imaging and regional distribution of basalt flows in the Faeroe-Shetland basin: Geophysical Prospecting, **51**, no. 3, 215–231, http://dx.doi.org/10.1046/j.1365-2478.2003.00364.x.